Electronic Supplementary Material (ESI) for Journal of Materials Chemistry A.

Supporting information:

Pseudocapacitive sodium storage in a brand new foveolate TiO_2@$MoSe_2$ nanocomposite enables high-performance Na-ion hybrid capacitors

Yang Su[1a], Yanfei Li[1a,b], Fei Qi[a], Shengen Gong[a], Guoduo Yang[a], Yihan Song[a], Xinglong Wu[a,b], Jingping Zhang[a], Haiming Xie[a] and Haizhu Sun[a*]

[a] *College of Chemistry, National & Local United Engineering Laboratory for Power Batteries, Northeast Normal University*
5268, Renmin Street, Changchun, 130024, P. R. China
b Center for Advanced Optoelectronic Functional Materials Research, and Key Laboratory of UV-Emitting Materials and Technology (Northeast Normal University), Ministry of Education,
5268, Renmin Street, Changchun, 130024, P. R. China

E-mail: sunhz335@nenu.edu.cn
*The Corresponding author.

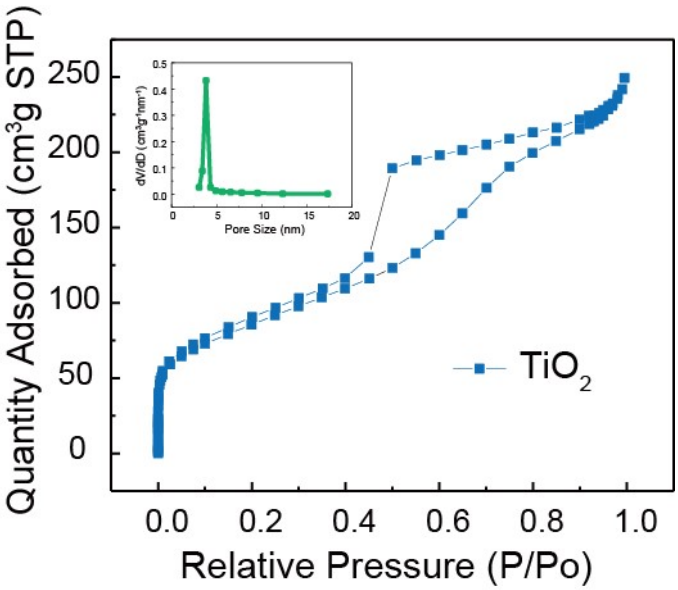

Fig. S1. Nitrogen sorption isotherms and pore size distribution of foveolate TiO_2.

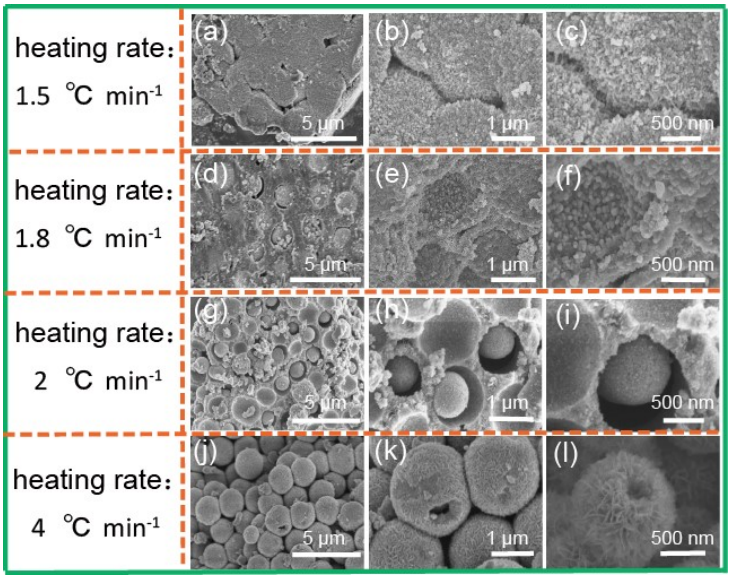

Fig. S2. Asymmetric Ostwald semi-mature mechanism investigation of foveolate TiO_2@$MoSe_2$ in different heating rates.

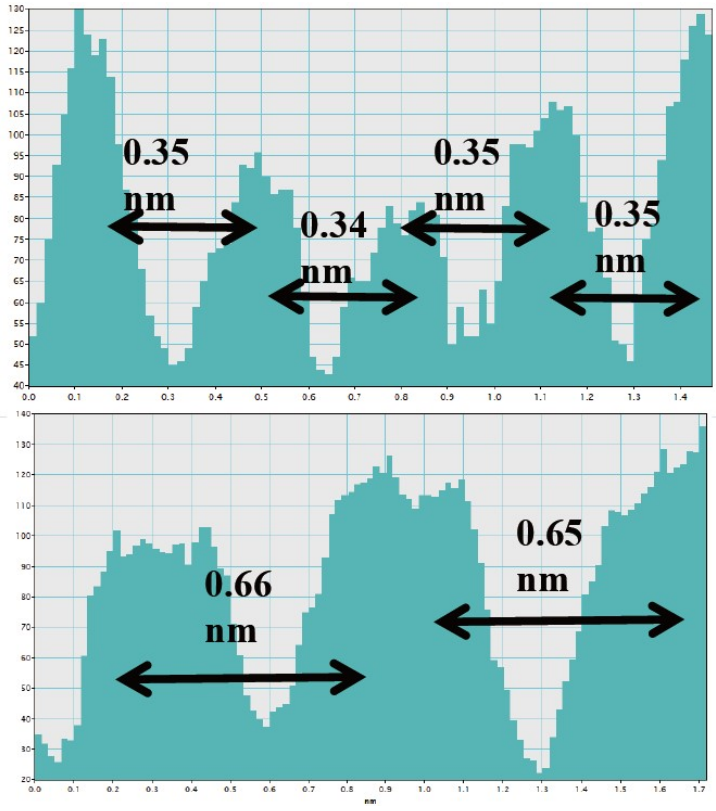

Fig. S3. (a, b) Line profiles of the d-spacing of the TiO_2 and $MoSe_2$ interlayers, indicating an average interlayer distance of 0.35 nm and 0.65 nm.

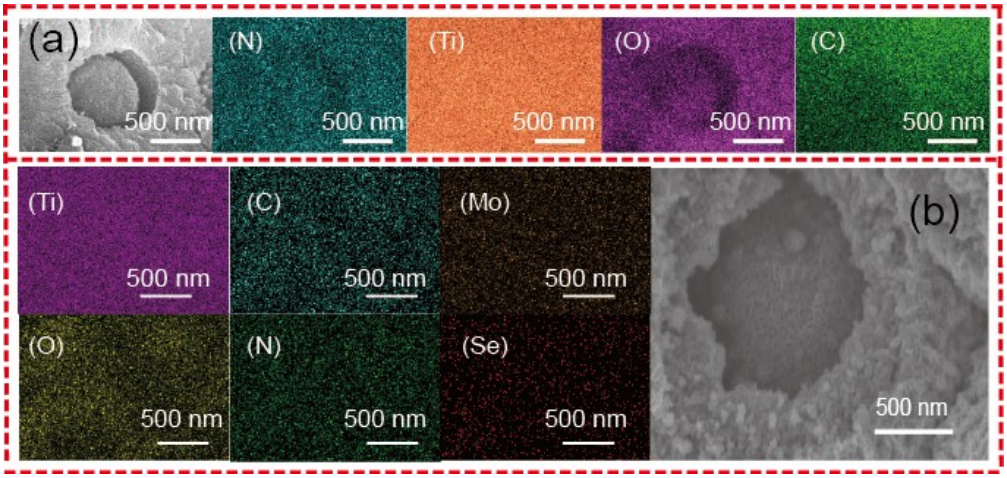

Fig. S4. (a) Element mapping images of TiO_2 (b) element mapping images of TiO_2@$MoSe_2$.

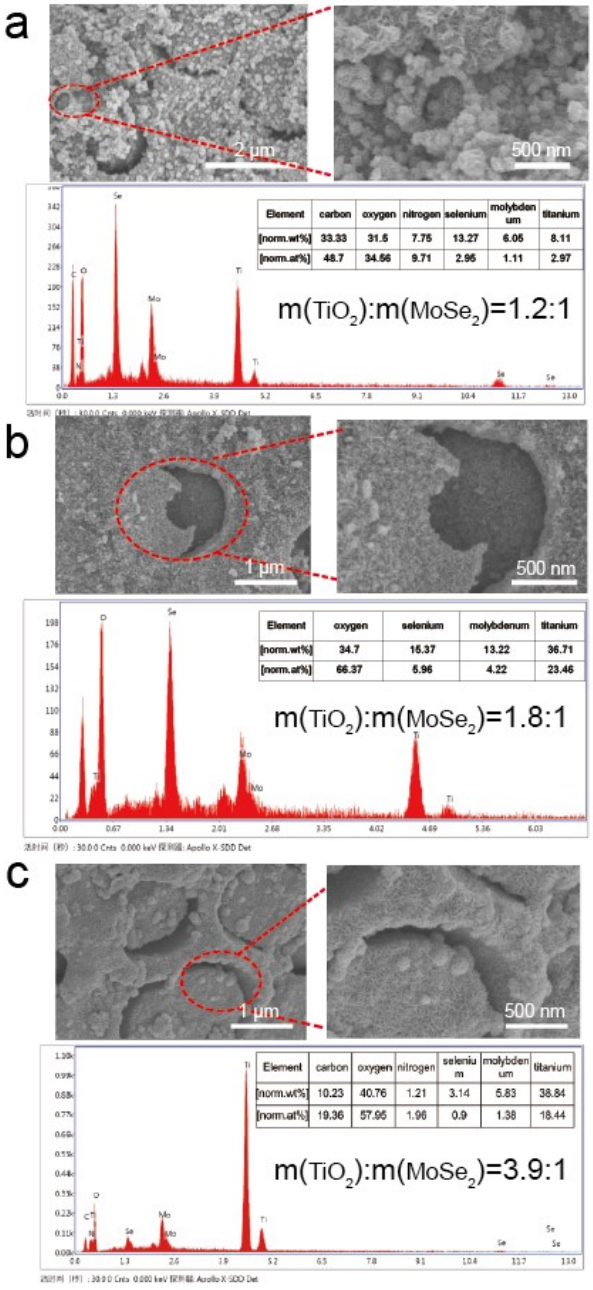

Fig. S5. Morphology characterization of TiO_2@$MoSe_2$ at 1.2:1, 1.8:1 and 3.9:1 mass ratio. Under 3.9:1 ratio, $MoSe_2$ grows uniformly on TiO_2, and the porous skeleton structure of foveolate TiO_2 is maintained.

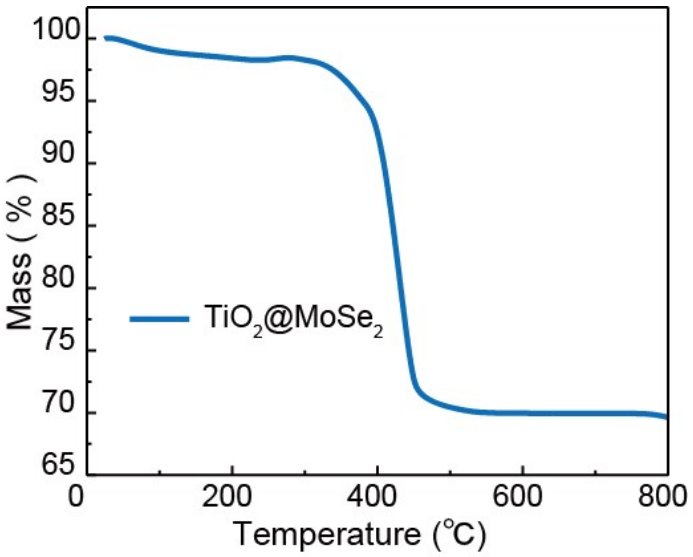

Fig. S6. TGA curve of TiO_2@$MoSe_2$ in air at a heating rate of 10℃ min^{-1}.

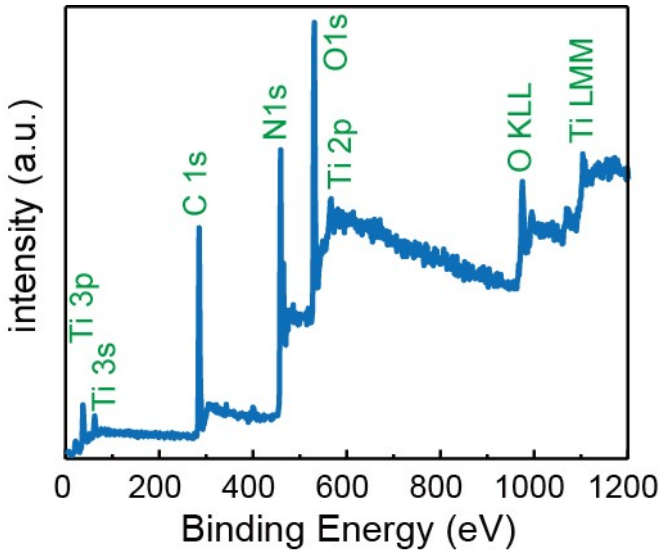

Fig. S7. XPS of TiO_2 (full spectrum).

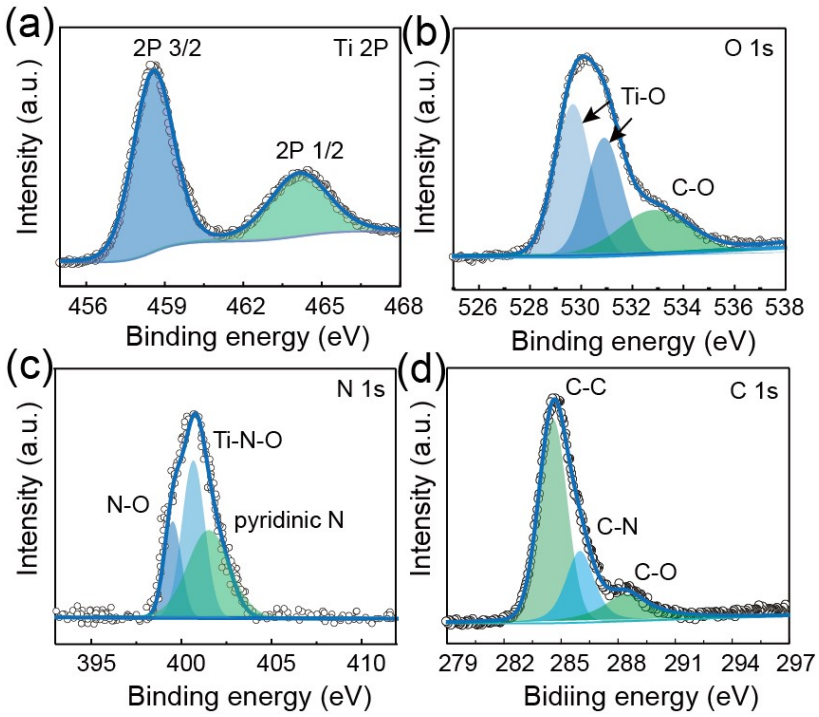

Fig. S8. XPS of the foveolate TiO_2, (a) Ti 2p; (b) O 1s; (c) N 1s; (d) C 1s.

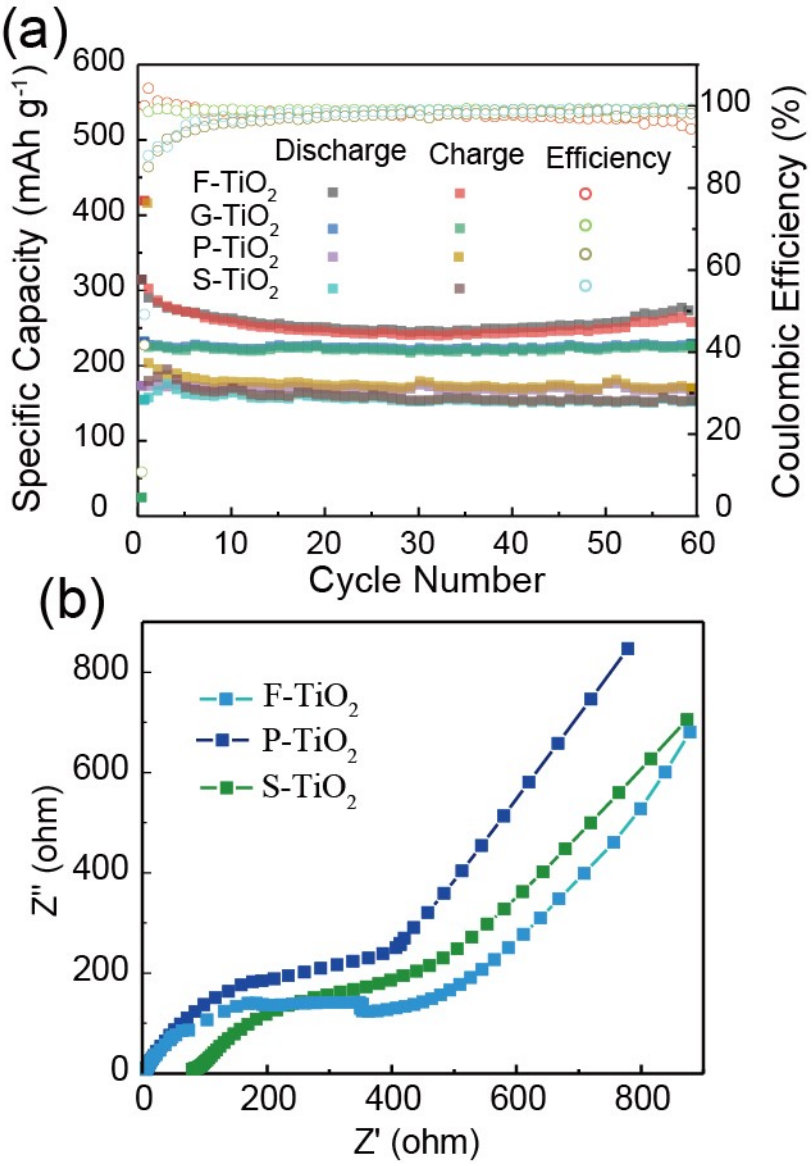

Fig. S9. (a) Capacity comparison of foveolate TiO_2 with different morphologies at the current density of 100 mA g^{-1}. (b) EIS plots of the TiO_2 with different morphologies.

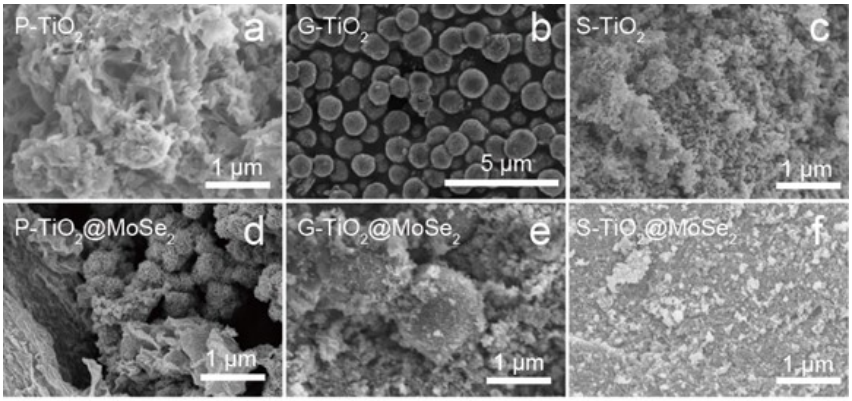

Fig. S10. SEM images of P-TiO_2 (a), G-TiO_2 (b), S-TiO_2 (c), P-TiO_2@$MoSe_2$ (d), G-TiO_2@$MoSe_2$ (e) and S-TiO_2@$MoSe_2$ (f).

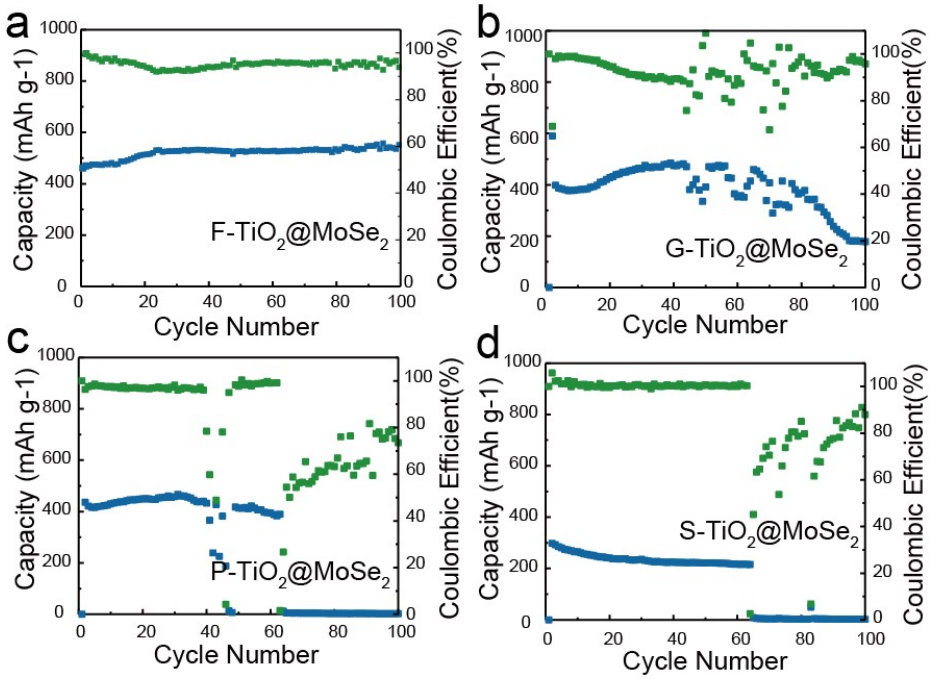

Fig. S11. Electrochemical cycling properties of TiO_2@$MoSe_2$ with different morphologies at 100 mA g^{-1}. (a) F-TiO_2@$MoSe_2$, (b) G-TiO_2@$MoSe_2$, (c) P-TiO_2@$MoSe_2$, (d) S-TiO_2@$MoSe_2$.

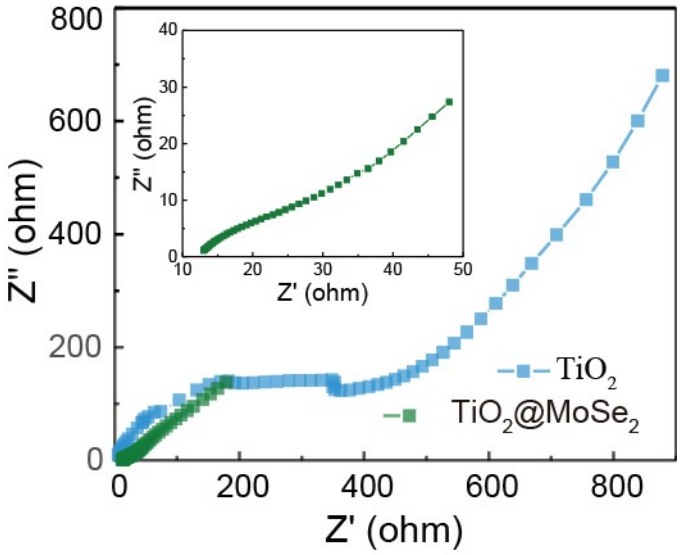

Fig. S12. EIS plots of the foveolate TiO_2 and TiO_2@$MoSe_2$.

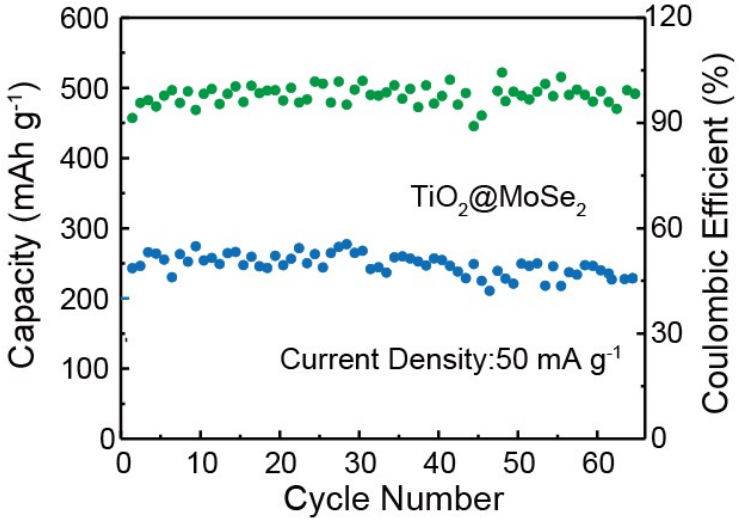

Fig. S13. Circulating performance of TiO_2@$MoSe_2$ at 50 mA g^{-1} under temperature of -15℃.

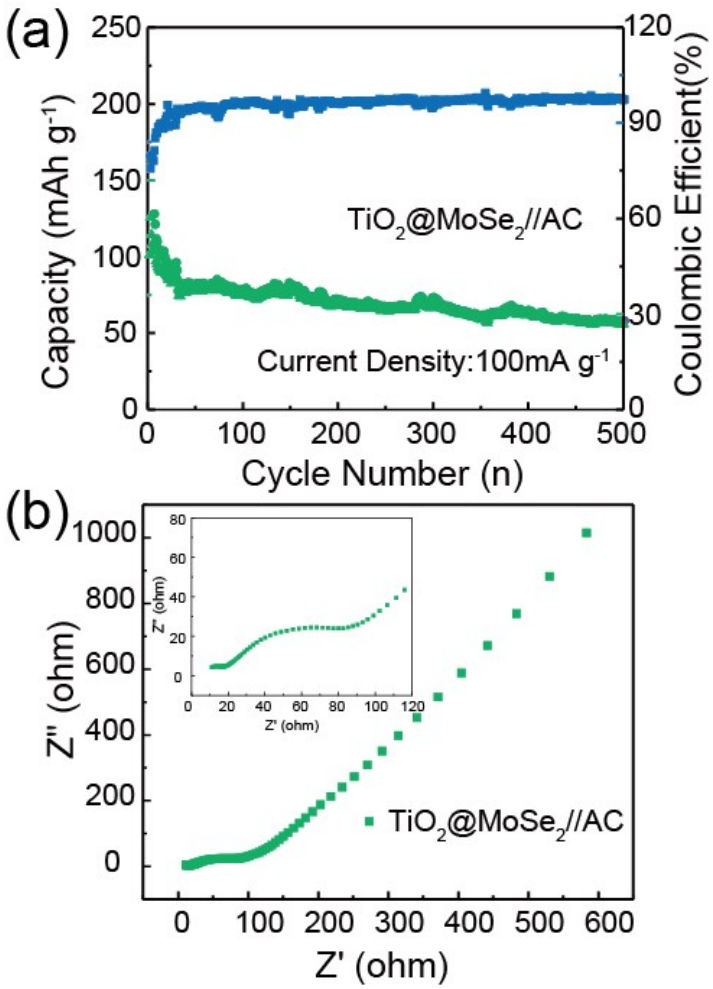

Fig. S14. (a) Circulating performance of SIHC (b) EIS plots of SIHC.

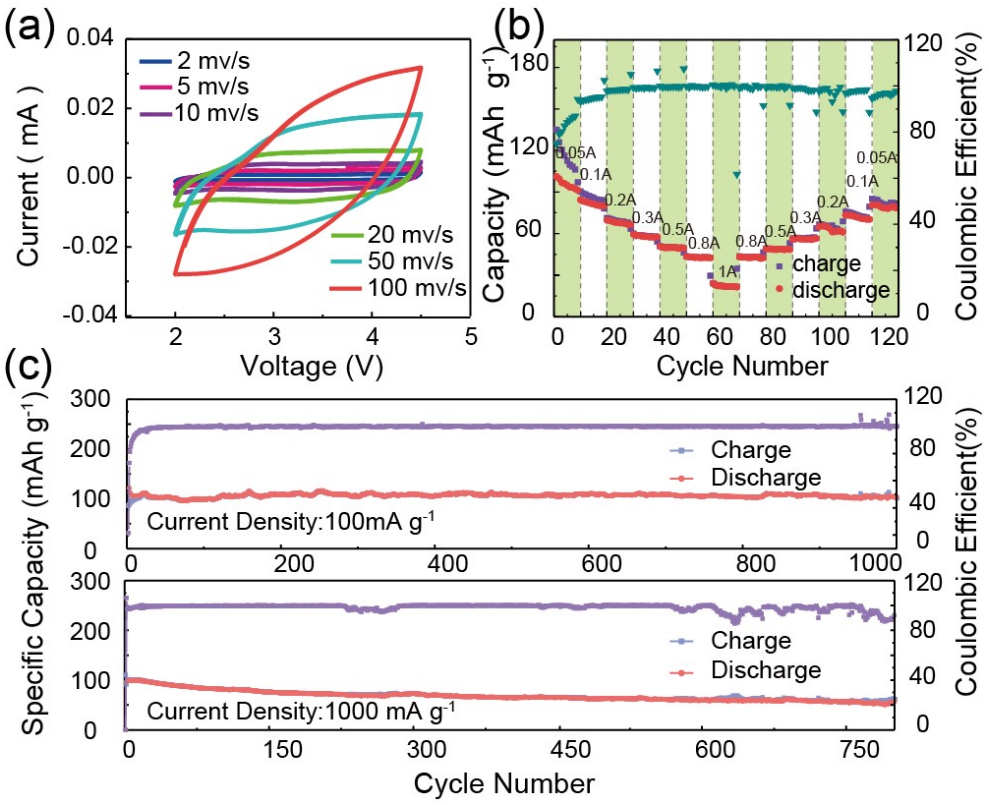

Fig. S15. (a) CV curve between 0.01 and 3.0 V of AC (b) the rate performances for AC at different rates. (c) Cycling stability of CV at 100 mA g^{-1} and 1000 mA g^{-1}.

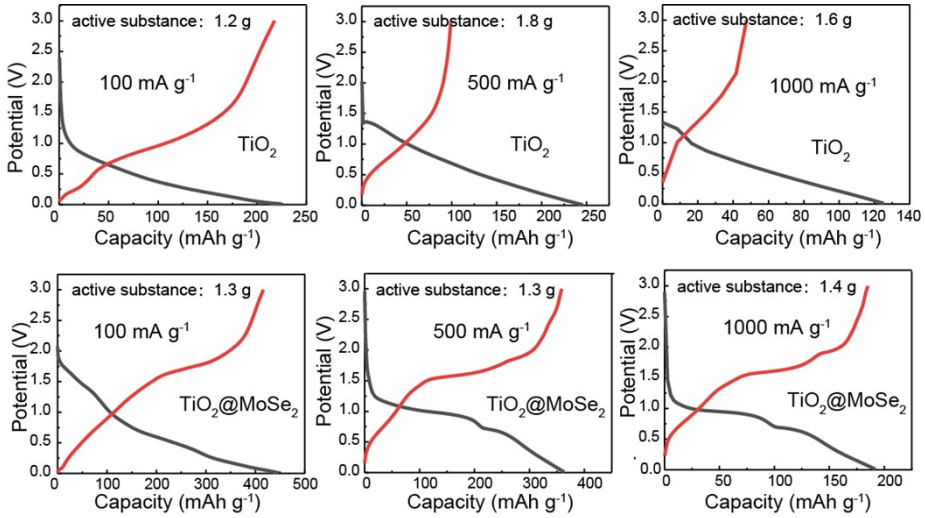

Fig. S16. Charge-discharge curves of foveolate TiO_2 and TiO_2@$MoSe_2$.

Table S1. Comparison of cycle and rate performance between foveolate TiO_2 and other reported TiO_2 anode materials.

	Initial coulombic efficiency	High rate capacity (1 C=336 mA g^{-1})	Cycling performance (mAh g^{-1})	References
Foveolate TiO_2 (F-TiO_2)	**96%**	**290 mAh g^{-1} at 100 mA g^{-1}, 208 mAh g^{-1} at 500 mA g^{-1}**	**158 mAh g^{-1}at 1000 mA g^{-1} after 1535 cycles;**	**This Work**
Globular TiO_2 (G-TiO_2)	73%	245 mAh g^{-1} at 100 mA g^{-1}	-	Controlled samples
Platelike TiO_2 (P-TiO_2)	42%	203 mAh g^{-1} at 100 mA g^{-1}	-	Controlled samples
Small particles of TiO_2 (S-TiO_2)	49%	179 mAh g^{-1} at 100 mA g^{-1}	-	Controlled samples
TiO_2 /C nanotubes	55.9%	242.5 mAh g^{-1} at 50 mA g^{-1}	153.9 mAh g^{-1} at 5000 mA g^{-1} after 14,000 cycles	[1]
Olive-like anatase TiO_2 /C	47.10%	267 mAh g^{-1} at 0.1 C, 110 mAh g^{-1} at 20 C	125 mAh g^{-1} at 10 C after 1000 cycles	[2]
R-TiO_{2-x} -S	No reported	264.8 mAh g^{-1} at 50 mA g^{-1}, 128.5 mAh g^{-1} at 10000 mA g^{-1} (~30 C)	264.8 mAh g^{-1} at 50 mA g^{-1}, 128.5 mAh g^{-1} at 10000 mA g^{-1} (~30 C)	[3]
Pinecone-like hierarchical anatase TiO_2 /C	43.20%	264.1 mAh g^{-1} at 0.1 C, 92.5 mAh g^{-1} at 15 C	108.2 mAh g^{-1} at 10 C after 2000 cycles	[4]
Nitrogen doped/carbon tuning yolk-like TiO_2	59.10%	242.7 mAh g^{-1} at 0.5 C, 115.9 mA h g^{-1} at 20 C	90.6 mA h g^{-1} at 25 C after 3000 cycles	[5]
TiO_2 mesocrystals	55%	151 mAh g^{-1} at 2000 mA g^{-1}	138 mAh g^{-1} at 500 mA g^{-1} after 200 cycles;	[6]

Porous carbon/TiO_2	No reported	173 mAh g^{-1} at 0.13 C, 68 mAh g^{-1} at 4.8 C	/	[7]
Oxygen vacancies evoked blue TiO_2 (B) nanobelts	41.50%	204.6 mAh g^{-1} at 0.25 C, 106.8 mAh g^{-1} at 12.5 C	80.9 mAh g^{-1} at 10 C after 5000 cycles	[8]
TiO_2@C Nanowires	No reported	197 mA h g^{-1} at 0.15 C	125 mA h g^{-1} at 3 C after 2500 cycles	[9]
Nitrogen-doped TiO_2 nanospheres	No reported	~200 mAh g^{-1} at 0.2 A g^{-1} , 147 mAh g^{-1} at 10 A g^{-1}	162 mA h g^{-1} at 1 A g^{-1} after 1000 cycles	[10]
TiO_2 @C nanosheets	No reported	264.9 mAh g^{-1} at 100 mA g^{-1}	92.9 mAh g^{-1} at 5 A g^{-1} after 4000 cycles	[11]

Table S2. Comparison of the initial Coulomb efficiencies of foveolate TiO_2 and other reported TiO_2 anode materials in different electrolytes.

	Initial coulombic efficiency	Electrolyte	References
Foveolate TiO_2 (F-TiO_2)	**96%**	**1 M $NaClO_4$, EC/PC (1:1), 5% FEC**	**This Work**
Globular TiO_2 (G-TiO_2)	73%	**1 M $NaClO_4$, EC/PC (1:1), 5% FEC**	Controlled samples
Platelike TiO_2 (P-TiO_2)	42%	**1 M $NaClO_4$, EC/PC (1:1), 5% FEC**	Controlled samples
Small particles of TiO_2 (S-TiO_2)	49%	**1 M $NaClO_4$, EC/PC (1:1), 5% FEC**	Controlled samples
TiO_2 /C nanotubes	55.9%	1 M $NaClO_4$, DMC/EC/EMC (1:1:1), 5% FEC	[1]
Olive-like anatase TiO_2 /C	47.10%	1 M $NaClO_4$, PC, 5%FEC	[2]
Pinecone-like hierarchical anatase TiO_2 /C	43.20%	1 M $NaClO_4$, PC, 5% FEC	[4]
Nitrogen doped/carbon tuning yolk-like TiO_2	59.10%	1 M $NaClO_4$, PC, 5% FEC	[5]
TiO_2 mesocrystals	55%	1 M $NaClO_4$, PC	[6]

Oxygen vacancies evoked blue TiO_2 (B) nanobelts	41.50%	1 M $NaClO_4$, PC, 5% FEC	[8]

References List:

1. H. He, Q. Gan, H. Wang, G.-L. Xu, X. Zhang, D. Huang, F. Fu, Y. Tang, K. Amine and M. Shao, Nano Energy, 2018, 44, 217-227.
2. J. Chen, Y. Zhang, G. Zou, Z. Huang, S. Li, H. Liao, J. Wang, H. Hou and X. Ji, Small, 2016, 12, 5554-5563.
3. H. He, D. Huang, W. Pang, D. Sun, Q. Wang, Y. Tang, X. Ji, Z. Guo and H. Wang, Adv. Mater., 2018, 30, 1801013.
4. J. Chen, G. Zou, H. Hou, Y. Zhang, Z. Huang and X. Ji, J. Mater. Chem. A, 2016, 4, 12591-12601.
5. Y. Zhang, C. Wang, H. Hou, G. Zou and X. Ji, Adv. Energy Mater., 2017, 7, 1600173.
6. W. Zhang, T. Lan, T. Ding, N.-L. Wu and M. Wei, J. Power Sources, 2017, 359, 64-70.
7. J. Lee, Y.-M. Chen, Y. Zhu and B. D. Vogt, ACS. Appl. Mater. Interfaces., 2014, 6, 21011-21018.
8. Y. Zhang, Z. Ding, C. W. Foster, C. E. Banks, X. Qiu and X. Ji, Adv. Funct. Mater., 2017, 27, 1700856.
9. Y. Wang, N. Li, C. Hou, B. He, J. Li, F. Dang, J. Wang and Y. Fan, Ceram Int., 2020, 46, 9119-9128.
10. S. Liu, Z. Cai, J. Zhou, A. Pan and S. Liang, J. Mater. Chem. A, 2016, 4, 18278-18283.
11. Q. Zhang, H. He, X. Huang, J. Yan, Y. Tang and H. Wang, Chem. Eng. J, 2018, 332, 57-65.